Advanced Robotics, 2015
http://dx.doi.org/10.1080/01691864.2015.1055799

Taylor & Francis
Taylor & Francis Group

FULL PAPER

Interaction forces beneath cuffs of physical assistant robots and their motion-based estimation

Yasuhiro Akiyama*, Yoji Yamada and Shogo Okamoto

Department of Mechanical Science and Engineering, Nagoya University, Nagoya, Aichi, Japan

(*Received 20 October 2014; revised 21 February 2015; accepted 8 May 2015*)

Most lower-limb physical assistant robots are fixed to wearers using cuffs. Hence, skin injuries beneath the cuffs are one of the major concerns of the users. A model that describes the relationship between the body posture and the interaction forces at the cuff was developed for use in assessing the risk of injury and improving user comfort. We measured the motion and interaction force beneath cuffs during the sitting and standing motions of subjects and a physical assistant robot which has been hardly reported thus far. Because of slippage and biomechanical motion, a traditional spring-damper model was found to be insufficient to describe the interaction forces associated with the measured motion of the cuffs. A parameter representing the motion or the knee joint angle was added to take into account these factors. Our model for estimation of the interaction forces using a spring, a damper, and the attitude of the lower leg fits the measured data especially well for the thigh cuff and is better than the traditional model. The applicability of this model was verified for several assist modes and wearers. The model was found to describe approximately 90% of the burden on the wearer, which reached a peak of approximately 60 N, the most hazardous condition. Having been validated for a commercial assistant robot, the model can be used to estimate the skin burdens beneath the cuffs without any force-sensitive elements.

Keywords: physical assistant robot; safety; sit–to–stand; human–robot interaction

1. Introduction

Physical assistant robots have been used mainly to assist in the rehabilitation of patients such as stroke survivors, under the supervision of physical therapists,[1–3] and trained workers and soldiers in special environments.[4] However, the range of applicability of physical assistant robots has been expanding in recent years. For example, improving the locomotion of elderly persons has become a new target application of lower-limb physical assistant robots.[5] When such assistant robots are used in daily living, a problem arises that had been considered somewhat minor, compared with high-risk problems such as falling. This problem is the occurrence of skin injuries caused by the skin being repeatedly stretched or scratched by the cuffs used to fix the robot to human limbs. Such injuries easily occur in people who have weak skin, such as patients with cirrhosis.

Assistant robots apply interaction or supportive forces to the wearer through cuffs. When the ergonomic mismatch and imperfect adjustment between a human body and a physical assistant robot are not negligible, the interaction forces that can lead to skin injury increase.[6] The risk of skin injury increases with the magnitudes of these interaction forces and the frequencies with which they are applied.[7] Therefore, it is necessary to validate the contact safety of physical assistant robots through testing. Such safety measures have to be considered in accordance with ISO 13482,[8] which is a safety standard for personal care robots, including physical assistant robots.

Skin stretching caused by interaction forces between the skin and cuffs is largely unavoidable because the motion of a robotic single-degree-of-freedom (1-DOF) pin joint and the ergonomic rotation and translation of a human joint [9,10] are fundamentally different, although some researchers have studied an advanced mechanism to mitigate this human–robot kinematic mismatch.[11] The assessment and prevention of large interaction forces and discomfort that could lead to skin injury are important to the safe use of physical assistant robots. However, with commercial robots, it is not easy to measure such forces or skin deformations beneath the cuffs. Direct measurement of skin deformation or interaction forces is needed for this purpose. Esmaeili et al., for example, suggested a relationship between the deformation energy of the skin and discomfort.[12] Other studies have used force sensors to measure interaction forces between the skin and fixed parts of a robot, such as cuffs, during motion.[13,14] However, commercial robots are rarely equipped with sensors for measurement of interaction forces or skin deformations under the cuffs. Such measurements are typically only possible in a laboratory setting. Therefore, while it is necessary to avoid large interaction forces beneath

*Corresponding author. Email: akiyama-yasuhiro@mech.nagoya-u.ac.jp

the cuffs, most commercial robots lack sensors in their cuffs and are thus unable to measure the forces or deformations that occur.

One possible solution to this problem is to estimate the interaction forces between the cuffs and the skin using kinematic information about the robot, which is usually accurately measured. However, the interactions between the fixed parts of a robot and a user's skin, such as viscoelastic deformation and slippage, remain incompletely understood and modeled. Hence, it is necessary to tune the parameters of the force estimation model for each user, using a customized robot equipped with force sensors. Once such parameters are tuned, the model can be used to estimate interaction forces without force sensors. In this study, we adopted an experimental approach to estimate interaction forces beneath the skin. We first attempted to estimate the forces on the basis of the relative displacement between the cuff and skin, using a spring–damper model. However, because of slippage between the skin and cuff, the hysteresis of human motions, and the changes in the physical parameters with human motion, this model was found to be insufficient. To compensate for the effect of slippage, we introduced a body posture term that is related to the fixation condition of the cuff with changes in posture. Furthermore, to counteract the hysteresis effect, models to estimate interaction forces were built for two phases of human motion: the standing and sitting phases. Models such as these for estimating the interaction forces between robot cuffs and human skin, based on kinematic information that is generally available for commercial robots, will contribute to improving the safety of use of physical assistant robots.

2. Method

This experiment was conducted with the permission of the Institutional Review Board (IRB) of Nagoya University.

2.1. Apparatus

The motions of a physical assistant robot and wearers were measured at 100 Hz using a three-dimensional (3D) motion capture system (MAC 3D system, Motion Analysis Corporation, US). Markers for the motion capture system were placed on the left sides of the bodies of the robot and the wearers. Cluster markers were used at positions covered by the robot. A commercially available physical assistant robot[1] was used for the tests. All links were connected by 1-DOF joints, and the hip and knee joints were actuated. Figure 1 shows an overview of how the robot was fixed to a wearer using belted cuffs. The robot could support itself because the frame of the robot reached the ground when standing straight. The lengths of the thigh link and shank link could be changed in 15-mm increments and were adjusted for each subject. The positions of the rotation centers of the hip and knee joints were aligned manually.

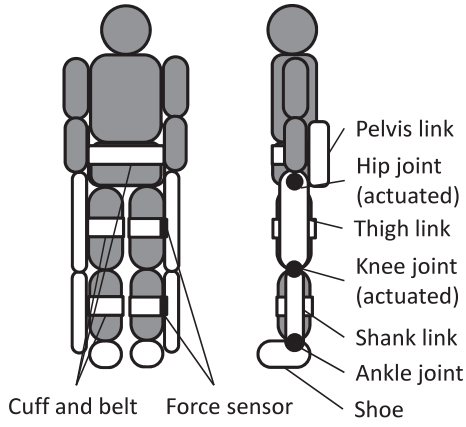

Figure 1. Overview of physical assistant robot.

The rotation center of the human was defined as the position of the great trochanter and lateral epicondyle.

The cuffs of the left leg were modified to measure the interaction forces, as shown in Figure 2. Two three-axis force sensors (US06-H5, Tech Gihan Co., Ltd., Japan), the outputs from which were sampled at 50 Hz, were attached to the base of cuff. The surface plate of each of the cuffs was then attached to the force sensors. The contact surface of the instrumented cuff, 65 × 90 mm in size, was covered with urethane. An artificial leather belt 50 mm wide was used to attach the cuff to the subject, and the belt was connected to the cuff. Thus, the measured interaction force included the force transferred through the belt. The instrumented cuff and belt were attached to the skin of the subject directory without any clothes.

In this experiment, three assist modes which include a non-assisted mode in which the robot was not actuated and the other two assist modes were used: a resistance compensation mode and a standing–sitting support mode. The resistance compensation mode cancels the resistance torque of the friction caused by the actuators and gears. The standing–sitting assist mode assists the sitting and standing motions by applying torque when the robot detects motions by installed encoders at the joints.

2.2. Protocol

This experiment was conducted with 10 healthy male volunteers who were between 22 and 24 years old (average age 23.1 years) and between 169 and 180 cm tall (average height 174.2 cm). The participants were not familiar with any types of physical assistant robots. The cuffs were fixed securely without causing discomfort to the subject. The tightening force (tension) of the belt was about 30–50 N. After the robot and markers were attached, three assist modes which include non-actuation case were tested for adaptation: non-assisted, resistance compensation, and standing–sitting support. The adaptation continued until the subject became

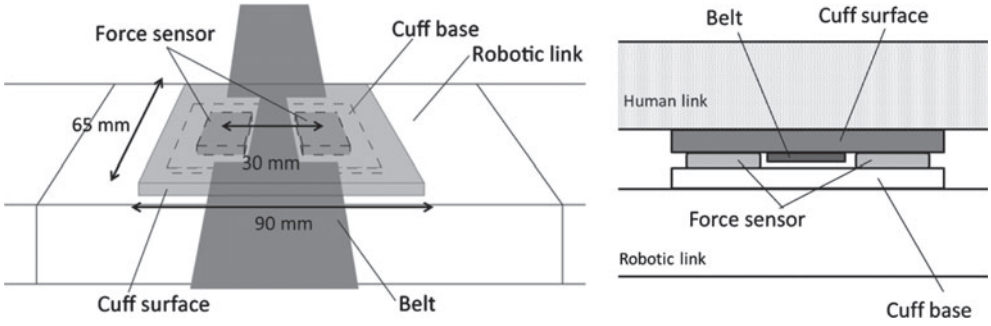

Figure 2. Structure of instrumented cuff (left: bird's eye view, right: sectional view).

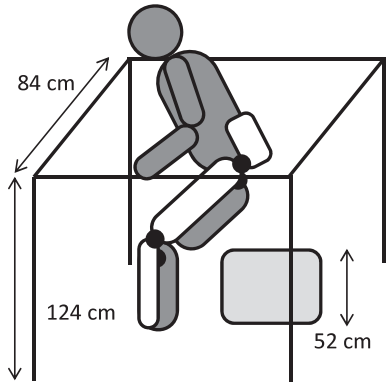

Figure 3. Conditions of sitting–standing motion.

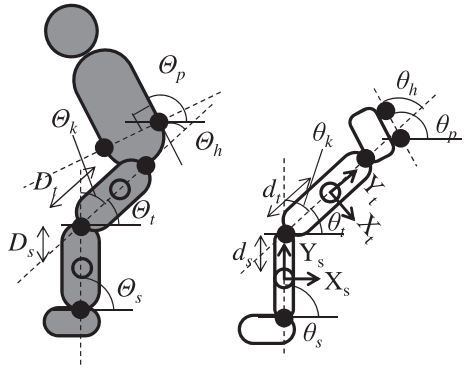

Figure 4. Geometry of attitude and position calculation.

comfortable. Then, the subject repeated sitting and standing 10 times for each assist mode. During the trial, the subject was ordered to grab the same position of the handrail. The sit–to–stand motion was selected because it is one of the fundamental motions of daily activities and because there is information about it in previous studies [15,16] that can be used for reference. Although the subject was informed about the assist mode of the next trial, the order of the assist modes was randomized to prevent order effect.

A chair and hand rails, which were fixed in position, were used to help with the motion. The chair was 52 cm tall, and the hand rails were set to a height of 124 cm, as shown in Figure 3. The horizontal spacing of the hand rails was 84 cm. The subjects were instructed to not move their feet and to minimize the variation in standing–sitting motions performed during the experiments.

2.3. Data processing

The motion capture markers were set so that the positions of more than two points of each link (pelvis, thigh, and lower thigh) were traced in the sagittal plane, with markers at each joint center and at the pelvis. The position of the hip joint of the wearer was calculated from markers on sacral and anterior superior iliac points on the spine.[17] External malleolus, lateral epicondyle, sacral vertebra, and anterior superior iliac spine locations were determined on the basis of palpation as the positions of markers on the subject. Markers were also placed at the centers of the ankle, knee, and hip joints on the robot. In addition, two markers were placed on the median line of the pelvis.

The angle of each link was defined using two markers for each link, and the angle of each joint was defined as the angle between neighboring links. The relative displacement of the cuff, which was defined as the distance between the cuff of the robot and its initial position of the subject, was calculated as follows. The initial cuff position was first fixed to the coordinates of each link. The cuff position was then traced by monitoring the position of each link.

Figure 4 shows the geometry of the angle and cuff distances. The coordinate system of the interaction forces matched that of the robotic links because force sensors were fixed to each robot's link. The origin of each coordination system is located at the center of each cuff, i.e. the center of two force sensors. The coordinate directions of each cuff were $\mathbf{X_t}$, $\mathbf{Y_t}$, $\mathbf{X_s}$, and $\mathbf{Y_s}$. In this figure, Θ_p, Θ_t, and Θ_s represent the angles of the human links (pelvis, thigh, and shank, respectively); Θ_h and Θ_k represent the angles of the human joints (hip and knee, respectively); $\theta_p, \theta_t, \theta_s, \theta_h$, and θ_k represent the respective angles of the robot; D_t and D_s represent the distances between the human knee joint and thigh or shank cuff, respectively; and d_t and d_s represent the distances between the robotic joint and cuffs, respectively.

Data on the link attitude and position, joint angle, relative displacement of the cuff, and interaction force were filtered with a linear-phase finite-impulse response (FIR) low-pass filter with a cutoff frequency of 2 Hz and a filter order of 30. The whole motion was separated into the sitting and standing phases. When the phases were separated, the edge of each phase was trimmed to ignore the effect of the static phase, i.e. still standing and sitting postures. One percent of the motion range for the robotic knee joint was used to trim the edge of each motion.

3. Results

This section summarizes the results obtained for the non-assisted mode, analyzed for the purpose of building kinematic models to estimate the interaction forces at the cuffs. The effect of each mode is discussed in Section 5.

3.1. Motion of subjects

Table 1 presents the results of a comparison of the pace of motion of each subject, conducted to verify the stability of the motion. The pace of motion was highly individual, but stable for almost all subjects. Figures 5–7 compare the changes in the angles of the links for each subject. The temporal sequence data were normalized by the length of the motions of the sitting and standing phases. All links became 90° when the subject stood erect, and forward tilting increased the link angle.

During the motion of sitting phase, the angle of the thigh link decreased with the flexion of the knee joint. At the same time, for many subjects, the lower thigh angle remained more than 90°, which means that the link was slightly bent forward. On the other hand, the pelvises of all subjects were bent backward at the end of sitting.

The trends for the motion of the standing phase were almost the opposite of those for the motion of the sitting phase, except for the early standing phase. Typically, when a subject stood up from the chair, the lower thigh and pelvis first bent forward to move the center of gravity forward. These sitting–standing motion patterns of the subjects corresponded to a general motion pattern that has been described in previous studies.[18,19]

3.2. Relative displacement between human limbs and robotic cuffs at cuff position

Because of the mismatch between the subject and the robot, which is the result of both the adjustment problem and the ergonomic motion, the position of the rotation center differs between the subject and the robot. Thus, a mismatch of the trajectory of the initial cuff position between the subject and the robot occurs, depending on the flexion of the knee joint. Figure 8 shows the initial, middle, and final postures of the subject and the robot. This figure clearly shows the relative motion, as described below.

Table 1. Average duration of motion of each subject.

Subject no.	Sitting pace [s]	± SD	Standing pace [s]	± SD
1	2.7	0.2	2.6	0.2
2	2.0	0.1	2.1	0.1
3	4.2	0.1	3.5	0.2
4	1.5	0.1	1.4	0.1
5	1.8	0.1	1.5	0.1
6	2.2	0.2	2.3	0.1
7	2.6	0.4	2.5	0.3
8	1.4	0.1	1.7	0.1
9	1.9	0.1	2.0	0.2
10	1.8	0.2	1.7	0.2

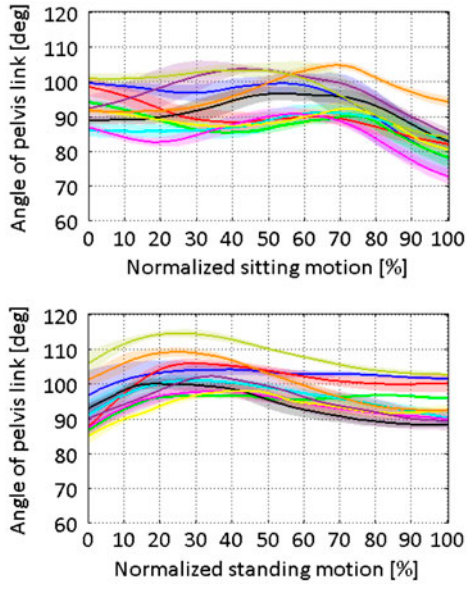

Figure 5. Change in θ_p of each subject during phases (top: sitting, bottom: standing).

3.2.1. Variance of the cuff position between subjects

Because of the limited accuracy of the manual alignment process and the difference of physical frame among individuals, the relative position of the cuff differs initially from one subject to another. This difference remains even after the motion becomes stable. Figures 9 and 10 illustrate the differences in the cuff positions of different subjects. In these graphs, the coordinates are fixed to the robotic thigh and shank link. The direction of the vertical axis matches the longitudinal axis of each link. The origin of this coordination system is the center of the robotic knee joint. The symbols indicate the trace of the position of the cuff at the initial setting along the center axis of human limb. The symbols for the standing posture are filled, and those for the sitting posture are not. The circles represent the motion of the sitting phase, and the squares represent the motion of the standing phase. The symbols of different colors represent the different subjects.

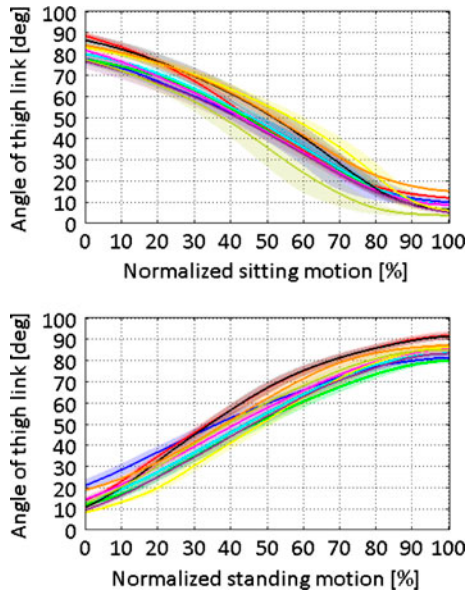

Figure 6. Change in θ_t of each subject during phases (top: sitting, bottom: standing).

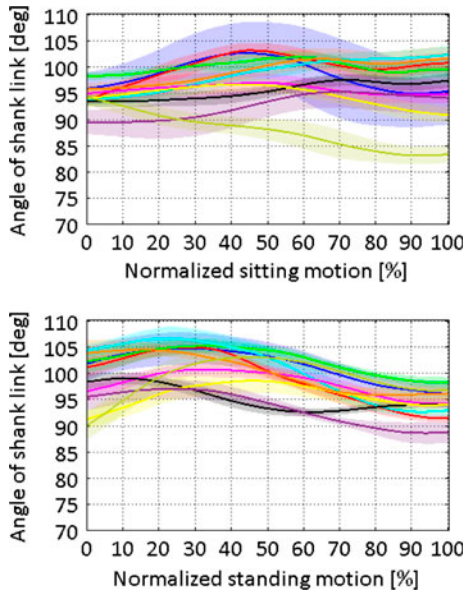

Figure 7. Change in θ_s of each subject during phases (top: sitting, bottom: standing).

Initially, because of the differences in the thigh lengths of the subjects, the nominal alignment point for the thigh cuff was (0, 200) for most of the subjects and (0, 230) for two of the subjects (represented by yellow and black symbols). In the sitting posture, the cuff position moved leftward and upward for many of the subjects, meaning that the subjects' limbs moved forward and upward from the robotic cuffs. However, the amounts of relative motion, indicated by the distances between the filled symbols and the blank symbols, differed among the subjects, and the relationship between initial misalignment and relative motion is not clear. Although initial misalignment might affect the relative motion between a subject's limb and a robotic cuff, there are many other factors, such as the shape of the subject's limb, muscle tension, and kinematic parameters of the skin and tissue, that influence the relative motion. The complex interaction between these factors should be analyzed and modeled carefully in another study to identify the effect of each factor.

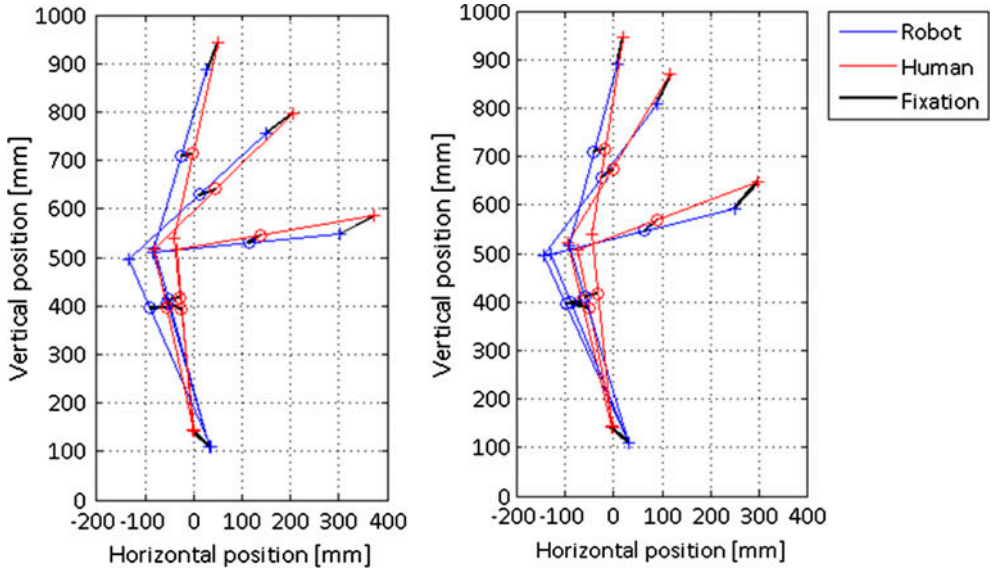

Figure 8. Postures of human and robot (left: sitting, right: standing).

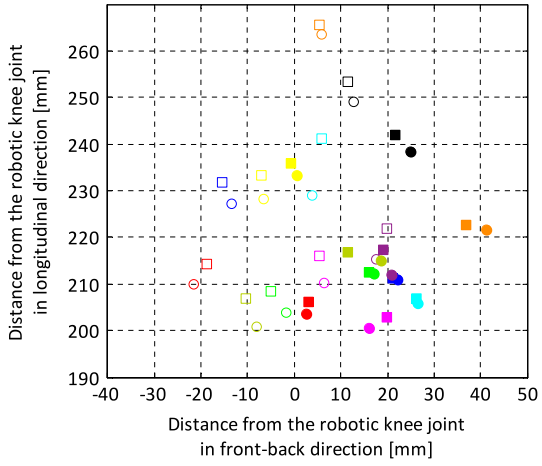

Figure 9. The positions of thigh cuffs from the center of the robotic knee joint. (The origin of the coordinate system is the robotic knee joint. Negative direction represents forward direction. Filled symbols represent the standing posture, and others represent the sitting posture. Each color represents a different subject.)

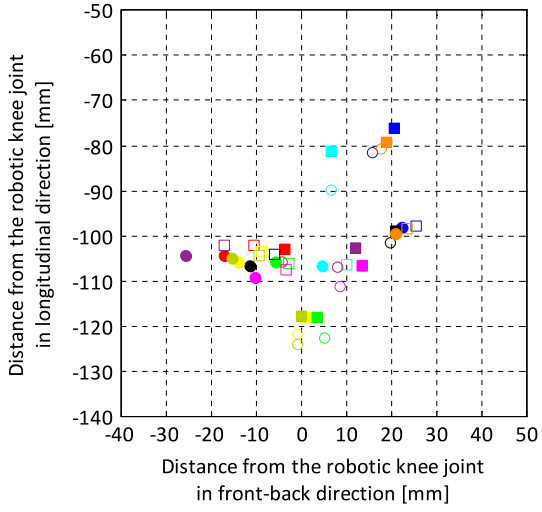

Figure 10. The positions of shank cuffs from the center of the robotic knee joint. (The origin of the coordinate system is the robotic knee joint. Negative direction represents forward direction. Filled symbols represent the standing posture, and others represent the sitting posture. Each color represents a different subject.)

3.2.2. *Relative displacement between the human thigh and thigh cuff over time*

The relative displacements between the subjects' thighs and the robotic thigh cuff were compared. Figure 11 shows the average relative displacements and their standard deviations (SD) for all subjects. The SD, which represents individual differences, increased during sitting motions and decreased

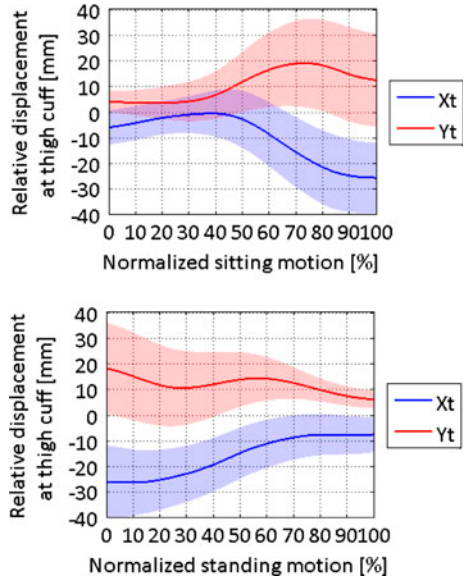

Figure 11. Relative displacement between human and robot at the position of the thigh cuff (top: sitting, bottom: standing).

during standing motions, which means that the individuality of the subjects was more pronounced in the sitting posture. The thigh link of the robot moved backward ($\mathbf{X_t} < 0$) and in the distal direction $\mathbf{Y_t} > 0$) with respect to the thigh of the subject during the sitting motion. These motions indicate that the robotic thigh link moved downward from the subject's thigh. When standing straight, the robot supported itself through its frame. However, the weight of each robotic link was applied to the subject through cuffs, with the posture becoming a half-crouching position. Thus, the robotic thigh link might have hung down from the thigh of the subject because of its weight.

The trend for the motion of the standing phase was not the reverse of that for the motion of the sitting phase. The relative displacement decreased gradually during motion of the standing phase. In addition, the cuff might have slipped, because the range of the relative displacement was too large to be the result of skin deformation.

3.2.3. *Relative displacement between the human shank and shank cuff over time*

Figure 12 shows the relative displacement between the subjects' shanks and the robotic shank cuff. As with the thigh cuff, the differences from one subject to another were more pronounced in the sitting posture. The robotic shank link moved forward ($\mathbf{X_s} > 0$) and in the proximal ($\mathbf{Y_s} < 0$) direction with respect to that of the subject when sitting. The motion of the shank link should be related to that of the thigh link because the two links are connected at the knee joint. Therefore, the thigh link may push the shank link forward, leading to motion in the $\mathbf{X_s} > 0$ direction, in

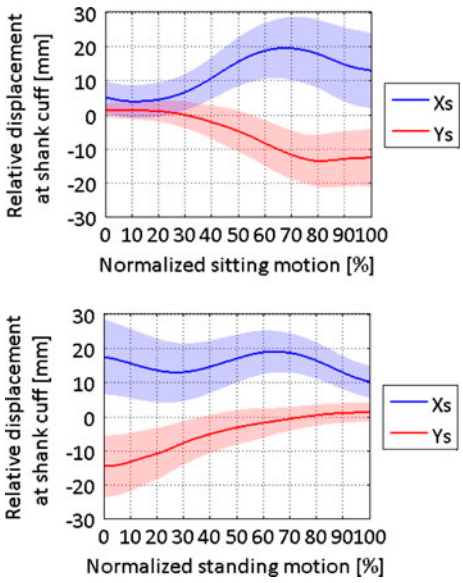

Figure 12. Relative displacement between human and robot at the position of the shank cuff (top: sitting, bottom: standing).

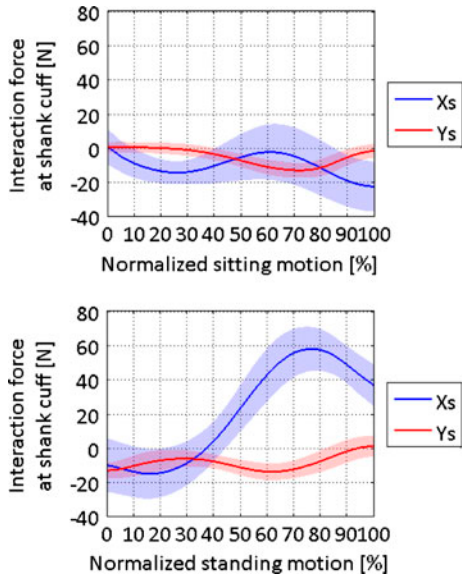

Figure 13. Interaction force between human and robot at shank cuff (top: sitting, bottom: standing).

the middle and later parts of the motion of the sitting phase. In addition, the change in the relative angle of the shank between the human and the robot influences the downward motion of the human shank, i.e. the motion in the $\mathbf{Y_s} < 0$ direction.

As this figure shows, the relative displacement of the shank cuff in the anteroposterior direction ($\mathbf{X_s}$) decreased in the early part of the motion of the standing phase because the lower thigh of the subject bent forward when the subject began to stand. This trend differed from that of the motion of the sitting phase. In addition, the range of the relative displacement was so large that it could not be described without the slippage of the cuff being the same as that of the thigh cuff.

3.3. Interaction force at cuffs

The relative motion at the cuff position produces an interaction force. Figures 13 and 14 show the average interaction forces at each cuff and their SD. These forces are the summation of both force sensors at a cuff. The interaction forces along $\mathbf{Y_t}$ increased with the sitting motion, which means that the robot hung down. This corresponded to the relative displacement of the cuff. In addition, the interaction forces at the shank cuff largely corresponded to the relative motion of the shank cuff. However, the interaction force of $\mathbf{X_s}$ became large late in the motion of the standing phase, which means that the shank of the subject was pushed from behind. When the subject pulled up the thigh of the robot, the shank link of the robot was pushed through the knee joint.

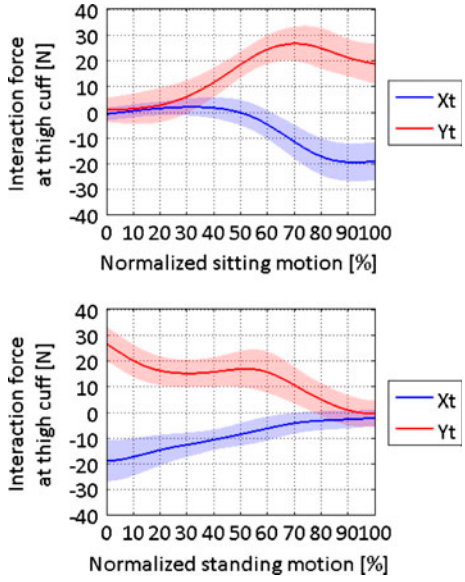

Figure 14. Interaction force between human and robot at thigh cuff (top: sitting, bottom: standing).

4. Fitting of physical model

4.1. Spring–damper model

Estimating and validating the interaction forces of a dynamic motion are difficult because of the unidentified biomechanical interactions between the skin and the cuff. In this study, a spring–damper model was used to describe the physical contact between the wearer and the robot. Viscoelastic deformation of the tissue [20,21] and fixed parts are collectively included in the parameters for the motion of the sitting and standing phases.

Table 2. $\overline{R}^2$ of spring–damper models.

	Sitting phase	Standing phase
$\mathbf{X_s}$	0.15	0.16
$\mathbf{Y_s}$	0.50	0.07
$\mathbf{X_t}$	0.80	0.58
$\mathbf{Y_t}$	0.37	0.22

Table 3. $\overline{R}^2$ of spring–damper and attitude models.

	Sitting phase	Standing phase
$\mathbf{X_s}$	0.44	0.89
$\mathbf{Y_s}$	0.50	0.09
$\mathbf{X_t}$	0.90	0.80
$\mathbf{Y_t}$	0.81	0.78

A spring–damper model described by the following formula was employed. A linear approximation was used because the displacements were assumed to be small. To determine the values of the parameters of this model, fitting was conducted using the least-squares regression method.

$$F(t) = kd(t) + cv(t) \tag{1}$$

The values of k and c, which represent the spring constant and viscosity, respectively, were determined after the values of F, d, and v, which represent the interaction force, the displacement between the cuff and the link, and its time-derivative value, respectively, were standardized for each subject. Table 2 lists the value of $\overline{R}^2$, which is the adjusted coefficient of determination, for each phase and part of the non-assisted mode. The results suggest that an inadequate $\overline{R}^2$ was obtained for almost all conditions, especially the motion of the standing phase. The spring–damper model cannot describe the actual interaction forces of the sitting and standing motions.

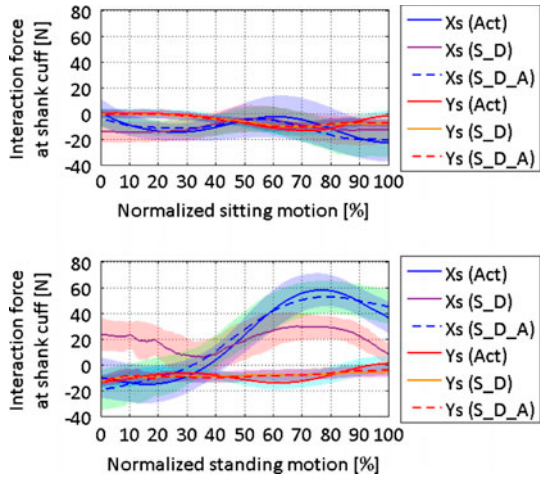

Figure 15. Comparison of actual interaction force (Act) and forces estimated from the models (S_D: spring–damper model, S_D_A: spring–damper and attitude model) at the shank cuff (top: sitting, bottom: standing).

4.2. Spring–damper and attitude model

4.2.1. Introduction of body attitude into the estimation model

A more advanced model was needed because the spring–damper model was found to be insufficient to describe the interaction forces associated with the motion observed. In general, the spring constant of skin tissue increases with displacement because the stretching range of skin tissue is limited.[22,23] However, a precipitous increase in the interaction forces against motion did not occur, except for $\mathbf{X_s}$ in the motion of the standing phase. Other factors that might affect the interaction forces are the slippage of the cuff and the shapes and diameters of the human thigh and shank. However, direct observation of the events that occur beneath the cuffs is difficult because this position is covered by the cuff. On the other hand, during the motion of the sitting and standing phases, the slippage direction of the cuff is probably consistent because the directions of human motion and gravity, which cause slippage, are fairly constant. In addition, the direction and magnitude of motion and gravity change with the attitude. Other parameters, such as the stiffness and shape of the subject's thigh and shank, also change with motion. Therefore, the angle of the robotic knee joint, which changes with the motion of the sitting and standing phases, was added as new parameter. This model is described by the following formula, using the knee angle θ_k and its coefficient a:

$$F(t) = kd(t) + cv(t) + a\theta_k(t). \tag{2}$$

Fitting of this model was performed in the same manner as for the spring–damper model. Table 3 lists the $\overline{R}^2$ value for each phase and part for the non-assisted mode. Except for $\mathbf{Y_s}$, the $\overline{R}^2$ values were substantially greater than those for the previous model. The $\overline{R}^2$ value for $\mathbf{Y_s}$ was apparently small because the average interaction forces along $\mathbf{Y_s}$ were small, nearly zero, across the entire body motions, whereas their variations were somewhat large. Under such conditions, $\overline{R}^2$ necessarily becomes small. In practice, we may not need to be concerned about the forces along $\mathbf{Y_s}$ because the risks of skin injuries caused by them are considered minuscule. The improvement in the estimation of the interaction forces is illustrated in Figures 15 and 16. According to these figures, the forces predicted by the spring–damper and attitude model fit the measured forces more accurately than those predicted by the spring–damper model. The improvement in the prediction of $\mathbf{X_s}$ is obvious.

To confirm the stability of the model, leave-one-out cross-validation was performed. As shown in Figure 17, the

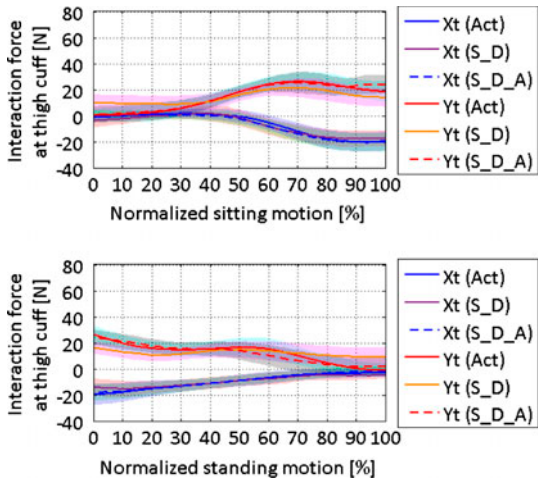

Figure 16. Comparison of actual interaction force (Act) and forces estimated from the models (S_D: spring–damper model, S_D_A: spring–damper and attitude model) at the thigh cuff (top: sitting, bottom: standing).

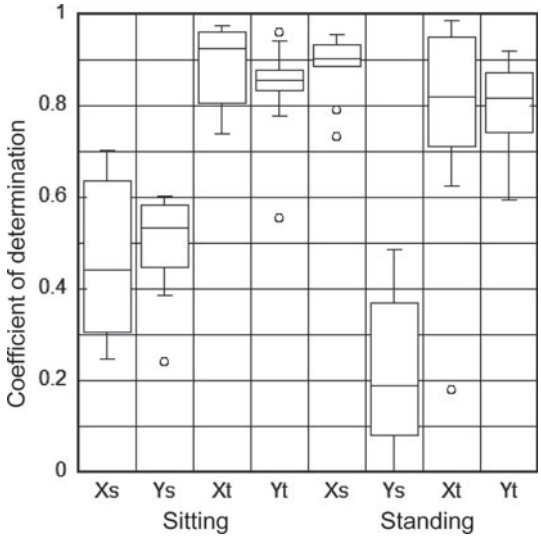

Figure 17. $\overline{R}^2$ of cross validation using spring–damper and attitude model for all subjects.

interaction forces at the thigh cuff have high $\overline{R}^2$ values, as does $\mathbf{X_s}$ in the motion of the standing phase. This trend corresponds to the $\overline{R}^2$ values listed in Table 3. However, certain outliers were observed. These are indicated by open circles in Figure 17.

4.2.2. *Regression coefficients of the model*

The physical model helps us to understand the phenomena that occur under the cuff and to specify each parameter of the model. To determine the contribution of each term of the model, the standard partial regression coefficients were compared as shown in Table 4. The value of k was larger

Table 4. Regression coefficients of spring–damper and attitude models.

		$\overline{R}^2$	k	c	a
Sitting phase	$\mathbf{X_s}$	0.44	0.64		−0.65
	$\mathbf{Y_s}$	0.50	0.75	0.28	0.12
	$\mathbf{X_t}$	0.90	0.46		−0.57
	$\mathbf{Y_t}$	0.81	0.29	0.19	0.76
Standing phase	$\mathbf{X_s}$	0.89	0.26		−0.87
	$\mathbf{Y_s}$	0.09			−0.32
	$\mathbf{X_t}$	0.80			−0.82
	$\mathbf{Y_t}$	0.78	0.35	0.17	0.75

Note: Statistically insignificant coefficients are not shown.

than that of c for almost all force components. In addition, $|a|$ was the largest parameter among the three coefficients. This suggests that the effect of the change in posture was greater than that of the relative displacement between the human limb and the robotic cuff and its velocity.

The interaction force generated by the relative displacement most likely results from the elasticity of human body tissues and cuff fixation parts. On the other hand, the force that results from the change in posture is the result of the slippage, muscle stiffness, and shape of the subject's thigh and shank.

A comparison of the coefficient values obtained from the regression showed that cases with high $\overline{R}^2$ values had coefficient values of the same order of magnitude. On the other hand, the coefficient values for cases with low $\overline{R}^2$ values, such as $\mathbf{Y_s}$ for both phases and $\mathbf{X_s}$ for the motion of the sitting phase, differed drastically from this trend. Therefore, we only discuss the coefficient values of the cases with high $\overline{R}^2$ values here. The coefficient values differed among the force components because of the differences in the fixation conditions, such as the tightening force, the thickness of the tissue, and the anisotropy of the fixation strength. The coefficient values of $\mathbf{X_t}$ changed between phases, in contrast to those of $\mathbf{Y_t}$. In particular, the value of k was not significant during the motion of the standing phase but was during the motion of the sitting phase. These changes in the coefficient values suggest that the fixation conditions changed between phases. In addition, for $\mathbf{X_s}$, both the coefficient values and the $\overline{R}^2$ value changed with the phase.

4.2.3. *Physical parameters of the estimated model*

The coefficients k, c, and a are dimensionless because they are based on normalized forces and postures. We translated these coefficients into the physical parameters, k', c', and a', which represent the coefficients of the elasticity, the viscosity, and the attitude elements, respectively. The physical parameters for cases with sufficiently high $\overline{R}^2$ values are listed in Table 5.

Table 5. Physical parameters of spring–damper and attitude models.

		k' [N/mm]	c' [Ns/m]	a' [N/deg]
Sitting phase	$\mathbf{X_t}$	0.20 to 0.98		−0.24 to −0.07
	$\mathbf{Y_t}$	0.19 to 0.72	0.63 to 1.84	0.16 to 0.37
Standing phase	$\mathbf{X_s}$	0.70 to 2.73		−1.58 to −0.46
	$\mathbf{X_t}$			−0.31 to −0.04
	$\mathbf{Y_t}$	0.28 to 0.76	0.05 to 0.21	0.12 to 0.27

Note: Statistically insignificant coefficients are not shown.

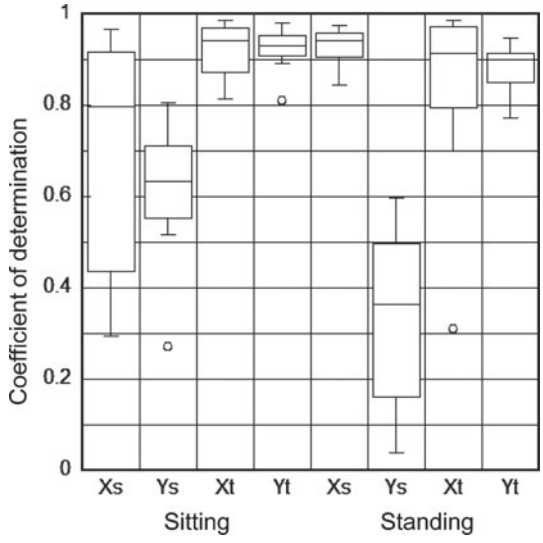

Figure 18. $\overline{R}^2$ of the spring–damper and attitude model tuned for each individual.

Although it is difficult to separate the coefficients by the skin, belt, and other components, some suggestions are provided in the literature. Clark measured the elastic coefficient of the antebrachial region of healthy humans.[24] The value obtained, 0.75 N/mm, is close to the value obtained in our calculations. Lundström measured the elastic and viscous coefficients of human fingers.[25] Their measurements indicated that k' was in the range of 1.5–5.6 N/mm and that c' was in the range of 1.0–2.8 Ns/m. Aso et al. measured the longitudinal elastic modulus of human thighs [26] and obtained values in the range of 0.7–2.8 N/mm. The k' and c' values obtained are close to those reported in previous studies, even though the region of the skin differs. This similarity in the results obtained suggests that the mechanical characteristics of the fixed parts of the physical assistance robot are primarily affected by the characteristics of skin tissue.

In practice, clothes must be worn underneath some robots. In these cases, interaction forces are affected by both the characteristics of the wearers and the characteristics of their clothes. Clothes are expected to reduce friction between a cuff and human skin, and the effect of slip increases. Therefore, the contributions of the spring and damper elements will change when clothes are worn.

5. Generality of the spring–damper and attitude model

5.1. Effect of individuality

5.1.1. Individual fitting improves the estimation

The differences in fixation conditions included differences in the area of contact, tightening force, thickness of tissue, friction coefficient, and shape of the fixation area. These parameters differed among individuals. If the low $\overline{R}^2$ of the spring–damper and attitude model is attributable to individuality, this model should more accurately fit each subject. Therefore, the model was separately fitted to the data for each subject. The results are summarized in Figure 18.

Although these results show an improvement in $\overline{R}^2$, there is still room for improvement in some force components. The results suggest that other factors, such as unevenness of the contact force, nonlinearity of the human tissue, and shape factors, may affect the contact between human skin and a cuff.

5.1.2. Individual difference in interaction force comes from the cuff position

We tested the individual differences in the maximum interaction forces applied to the cuffs because the residual individual differences might suggest the necessity of additional parameters that affect the interaction force. Figures 19 and 20 show the minimum and maximum interaction forces of each subject. Each subject is represented by a different color. The colors correspond with those used in other figures in this paper. The initial setting of the position of the cuff may be the main concern with respect to the residual parameters because it potentially affects the relative motion. However, as discussed previously, the cuff position in the standing or sitting postures did not appear to affect the relative motion of the cuff. Thus, the effect of differences in the cuff position can be reflected in the interaction force at the cuff.

The Tukey-Kramer method was used to determine whether the differences in the interaction forces of these subjects were significant. The maximum absolute values of the interaction force were compared because the interaction force affects discomfort and skin injury. As a result, it was hard to associate the pairs of the subjects whose interaction force differed significantly with the position of the thigh cuff, which was shown in Figure 9, in the $\mathbf{X_t}$ direction. In contrast, in the $\mathbf{Y_t}$ direction, the forces for the subjects represented by the black and yellow symbols, which were different in the direction of the longitudinal axis, were significantly greater than those of the other subjects. This difference most likely arose from the shape of the human thigh

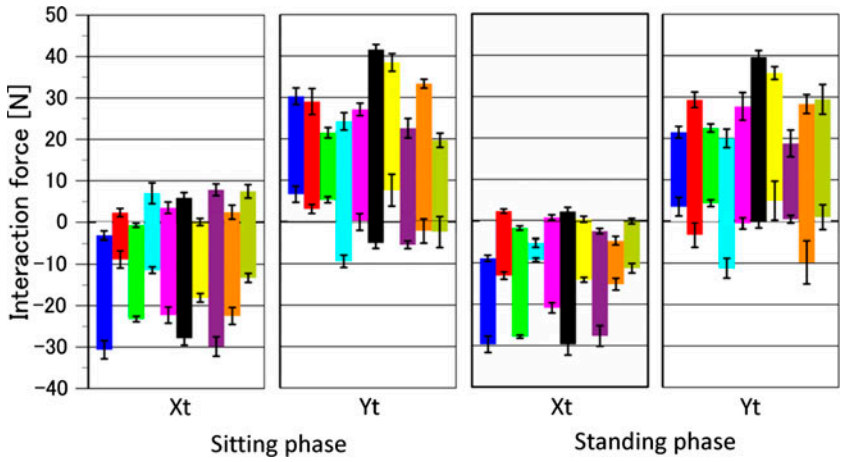

Figure 19. Range of interaction force at the thigh cuff.

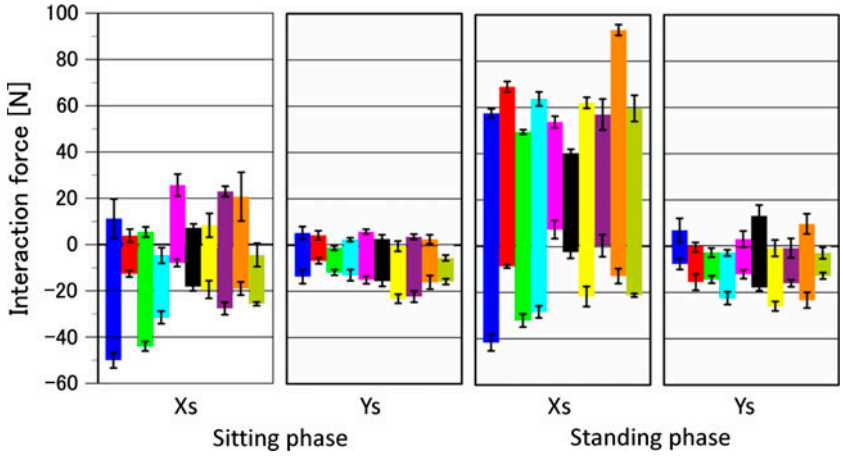

Figure 20. Range of interaction force at the shank cuff.

under the cuff. The diameter of the lower part of the thigh increases with the height, and the gradient becomes milder because of the shape of muscle. In this experiment, the thigh cuff was located 230 mm from the center of the knee joint on the subjects represented by the black and yellow symbols, which was 30 mm farther away than for the other subjects because of the different thigh lengths of the subjects. Thus, for those two subjects, the cuff might have been strongly fixed in the direction of the lower side because the shape of the human thigh became more cylindrical with increasing length. Although there were some pairs of subjects whose interaction forces differed significantly at the shank cuff, which was shown in Figure 10, it was difficult to associate these differences with the position of the cuff.

5.2. Effect of assist mode

The assist torque should change the sitting and standing motions and the interaction forces. We checked to ensure that our model was valid for the different assist modes.

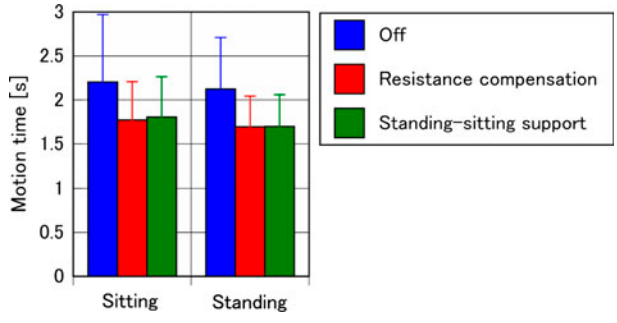

Figure 21. Motion time of each mode.

Figure 21 compares the lengths of the phases of each mode. The motion decreases with assistance. This suggests that the resistance torque prevents motion of the subject in the non-assisted mode. However, there was no difference between the two assist modes.

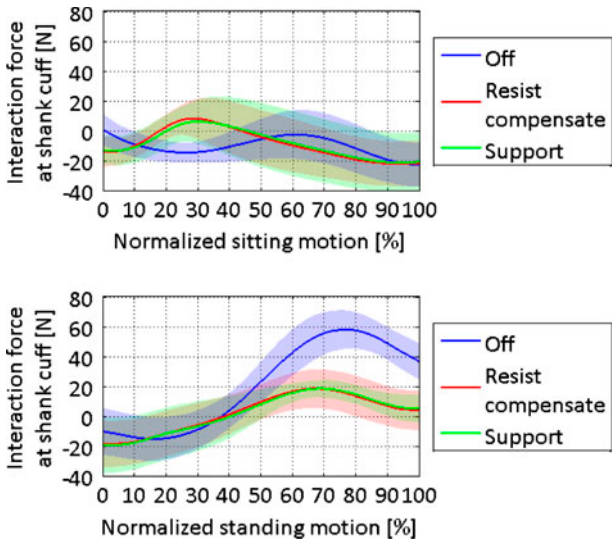

Figure 22. Interaction force of shank cuff in anteroposterior direction ($\mathbf{X_s}$) (top: sitting, bottom: standing).

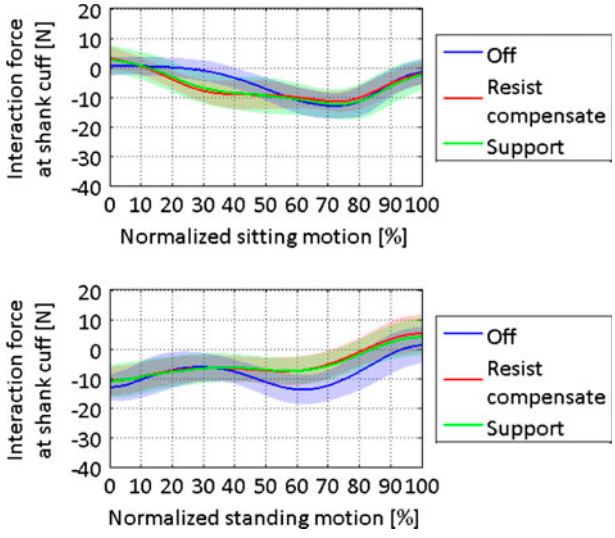

Figure 23. Interaction force of shank cuff in anteroposterior direction ($\mathbf{Y_s}$) (top: sitting, bottom: standing).

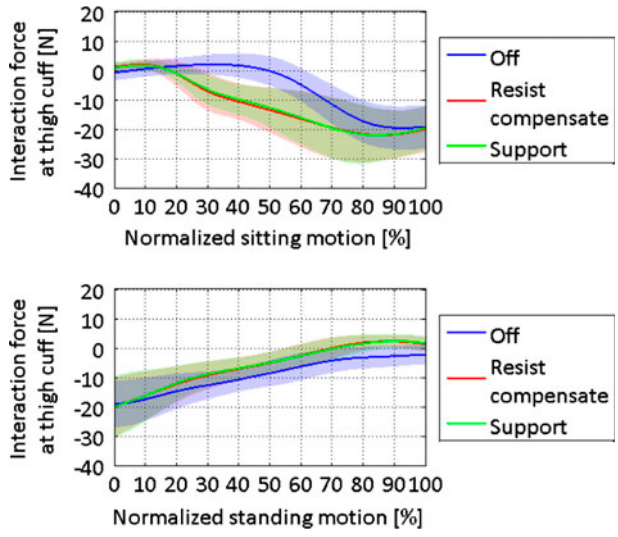

Figure 24. Interaction force of thigh cuff in anteroposterior direction ($\mathbf{X_t}$) (top: sitting, bottom: standing).

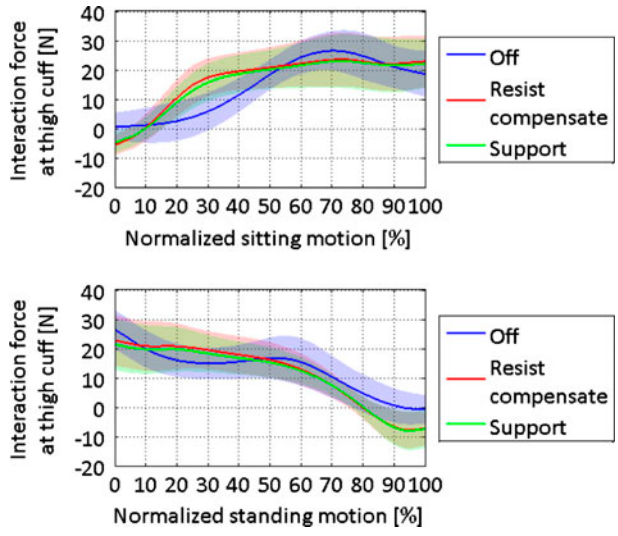

Figure 25. Interaction force of thigh cuff in anteroposterior direction ($\mathbf{Y_t}$) (top: sitting, bottom: standing).

Figures 22–25 compare the interaction forces at the cuffs. According to these figures, the interaction forces differed between the non-assisted and other modes, and the difference between two assist modes was small. These changes reflect the change in motion caused by the assist torque. For example, $\mathbf{X_s}$ in the motion of the standing phase differs drastically by mode, and the fact that the peak value of $\mathbf{X_s}$ decreases because of the change suggests that assist torque compensates for the mass and resistance that push the shank forward in the non-assisted mode.

To evaluate the changes in the fitting parameters, the $\overline{R^2}$ and coefficient values for each mode were compared, as shown in Tables 6 and 7. According to these tables and Table 4, there is a large difference between the non-assisted mode and the other modes. In particular, $\mathbf{Y_s}$ in the motion of the standing phase is completely different, although $\mathbf{Y_s}$ is considered insignificant, as described before. Therefore, this model should be tuned for each assist mode to obtain an adequate $\overline{R^2}$. In addition, a negative value of k was obtained for $\mathbf{Y_s}$, which is unrealistic and suggests the necessity of explicit consideration of assist torque when estimating kinematic parameters.

It seems strange that the two assist modes had no differences. However, this can be explained by the assumed motion speed of the assistance. The robot was designed to assist in rehabilitation, and the speed of its motion is suitable

Table 6. Coefficient values of spring–damper and attitude models in resistance compensation mode.

		$\overline{R}^2$	k	c	a
Sitting phase	$\mathbf{X_s}$	0.62	0.66	0.19	−0.69
	$\mathbf{Y_s}$	0.38	0.08	0.36	−0.47
	$\mathbf{X_t}$	0.91	0.20		−0.77
	$\mathbf{Y_t}$	0.76	0.33	0.19	0.79
Standing phase	$\mathbf{X_s}$	0.65	0.52		−0.85
	$\mathbf{Y_s}$	0.52			−0.76
	$\mathbf{X_t}$	0.86			−0.90
	$\mathbf{Y_t}$	0.84	0.21		0.84

Note: Statistically insignificant coefficients are not shown.

Table 7. Coefficient values of spring–damper and attitude models in sitting-standing support mode.

		$\overline{R}^2$	k	c	a
Sitting phase	$\mathbf{X_s}$	0.64	0.71	0.18	−0.72
	$\mathbf{Y_s}$	0.44	−0.10	0.32	−0.68
	$\mathbf{X_t}$	0.92	0.16		−0.82
	$\mathbf{Y_t}$	0.77	0.31	0.18	0.79
Standing phase	$\mathbf{X_s}$	0.71	0.49		−0.87
	$\mathbf{Y_s}$	0.61	−0.33		−1.08
	$\mathbf{X_t}$	0.85			−0.86
	$\mathbf{Y_t}$	0.85	0.23		0.82

Note: Statistically insignificant coefficients are not shown.

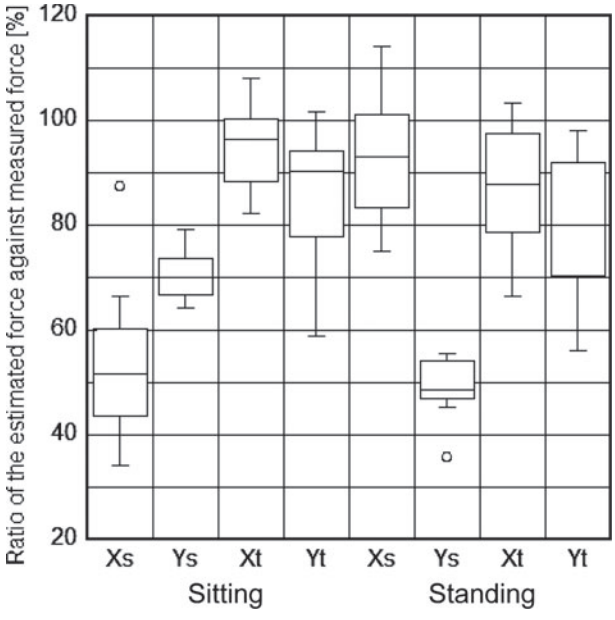

Figure 26. Ratio of the average peak force between the estimated and measured force.

for a stroke patient. The subjects in this study moved too quickly for assistance to work properly.

5.3. Estimation error and safety margin

The magnitude of the shear force applied to the skin is an indicator of the potential for skin injury.[7] Thus, an important requirement of the model was to be able to accurately estimate the amplitude of the interaction force. Figure 26 shows the ratio of the average peak force of each subject between the estimated interaction force and measured one. For the thigh cuff, for which the most critical shear forces were measured, the estimated force exerted at the thigh cuff, whose $\overline{R}^2$ was comparatively high, was within approximately 50–120% of the actual values. These differences should be taken into consideration by applying a safety margin to the prediction of the risk of skin injury by the robot.

6. Conclusions

The interaction forces at the cuffs of a physical assistant robot should not be substantially larger than the magnitudes required to facilitate motion while ensuring the safety and comfort of the user. However, it is difficult to estimate the interaction forces during actual motions because the frictional behaviors and human limb shapes at the cuff are not easily modeled. In this study, a spring–damper and attitude model was developed to describe the interaction forces during sitting and standing motions. The effects of factors that depend on the posture, such as slippage between the cuff and human skin, were successfully represented in this model by the addition of an attitude parameter that represents the relationship between motion and slippage. The goodness of fit of the model was evaluated using the adjusted coefficient of determination. The values of the spring constant k' and viscosity c' were found to be within their valid ranges, given the mechanical characteristics of the skin. The spring–damper and attitude model can, to a certain degree, estimate the interaction forces that occur during sitting and standing motions, despite differences from person to person.

The results suggest that the interaction force along $\mathbf{X_s}$ exceeds 60 N for the most hazardous conditions that can produce skin injury. Our model was able to describe approximately 90% of this maximum burden. It is important to note that the conditions under which this model can be applied should be carefully identified. However, the interaction forces can be estimated for an individual wearer from his or her motions, once the parameters are adjusted. Our model can be used to estimate signs of potential wounds of the skin even for commercial robots that do not have force sensing elements installed in the cuffs.

Funding

This study was conducted as a part of the 'Practical Applications of Service Robot Project,' which is directed by the New Energy

and Industrial Technology Development Organization (NEDO); JSPS KAKENHI [grant number 26750121].

Disclosure statement

No potential conflict of interest was reported by the authors.

Note

1. Because of contractual obligations, the name, manufacturer, and details of the assist algorithm cannot be mentioned, to avoid the evaluation of this particular robot.

Notes on contributors

Yasuhiro Akiyama received the BE degree in engineering from Tokyo Institute of Technology, Tokyo, Japan, in 2006, and the MS and the PhD degree in engineering from the University of Tokyo, Tokyo, Japan, in 2008 and 2011, respectively. Since then, he has been a postdoctoral researcher at Nagoya University, Nagoya, Japan. His main areas of research interests are mechanical safety, human–robot interaction, and manned space mission.

Yoji Yamada received a doctor degree from Tokyo Institute of Technology in 1990. He had been with Toyota Technological Institute, Nagoya, Japan, since 1983 and became an associate professor in the Graduate School of the Institute. In 2004, he joined Intelligent Systems Research Institute of National Institute of Advanced Industrial and Science Technology (AIST). In 2009, he moved to the Department of Mechanical Science and Engineering, Graduate School of Engineering, Nagoya University as a professor. Dr Yamada is a member of Robotics Society of Japan, and his current research interests include safety and intelligence technology in human/ machine systems, their robotic sensing and control.

Shogo Okamoto received MS and PhD degrees in information sciences in 2007 and 2010, respectively, from the Graduate School of Information Sciences, Tohoku University. Since 2010, he has been an assistant professor at the Graduate School of Engineering, Nagoya University. His research interests include haptics and human-assistive technology.

References

[1] Wier LM, Hatcher MS, Triche EW, et al. Effect of robot-assisted versus conventional body-weight-supported treadmill training on quality of life for people with multiple sclerosis. J. Rehabil. Res. Dev. 2011;48:483–492.
[2] Kawamoto H, Sankai Y. Power assist method based on phase sequence. Adv. Rob. 2005;19:717–734.
[3] Lapitskaya N, Nielsen J, Fuglsang-Frederiksen A. Robotic gait training in patients with impaired consciousness due to severe traumatic brain injury. Brain Inj. 2011;25:1070–1079.
[4] Zoss AB, Kazerooni H, Chu A. Biomechanical design of the Berkeley lower extremity exoskeleton (BLEEX). IEEE/ASME Trans. Mechatron. 2006;11:128–138.
[5] Yasuhara K, Shimada K, Koyama T, et al. Walking assist devices with stride management system. Honda R&D Tech. Rev. 2009;21:54–62.
[6] Akiyama Y, Yamada Y, Ito K, et al. Test method for contact safety assessment of a wearable robot -analysis of load caused by a misalignment of the knee joint. In: The 21st IEEE International Symposium on Robot and Human Interactive Communication; Paris; 2012 Sep. p. 539–544.
[7] Naylor PFD. The skin surface and friction. Br. J. Dermatol. 1955;67:239–246.
[8] ISO. Robots and robotic devices – safety requirements for personal care robots. International Organization for Standardization; 2014. Tech Rep ISO 13482:2014.
[9] Yamaguchi GT, Zajac FE. A planar model of the knee extensor mechanism. J. Biomech. 1989;22:1–10.
[10] Malosio M, Pedrocchi N, Vicentini F, et al. Analysis of elbow-joints misalignment in upper-limb exoskeleton. In: 2011 IEEE International Conference on Rehabilitation Robotics; Zurich; 2011 Jun. p. 1–6.
[11] Cempini M, Rossi SMMD, Lenzi T, et al. Self-alignment mechanisms for assistive wearable robots: a kinetostatic compatibility method. IEEE Trans. Rob. 2013;29:236–250.
[12] Esmaeili M, Gamage K, Tan E, et al. Ergonomic considerations for anthropomorphic wrist exoskeletons: a simulation study on the effects of joint misalignment. In: 2011 IEEE/RSJ International Conference on Intelligent Robots and Systems; San Francisco, CA; 2011. p. 4905–4910.
[13] Kao PC, Srivastava S, Agrawal SK, et al. Effect of robotic performance-based error-augmentation versus error-reduction training on the gait of healthy individuals. Gait Posture. 2013;37:113–120.
[14] Lewis CL, Ferris DP. Invariant hip moment pattern while walking with a robotic hip exoskeleton. J. Biomech. 2011;44:789–793.
[15] Reisman DS, Scholz JP, Schöner G. Differential joint coordination in the tasks of standing up and sitting down. J. Electromyogr. Kinesiol. 2002;12:493–505.
[16] Dionisio VC, de Biagi Curtarelli M, de Souza LAPS. Sitting movement in elderly subjects with and without Parkinson's disease: a biomechanical study. J. Electromyogr. Kinesiol. 2013;23:948–957.
[17] Bell AL, Pedersen DR, Brand RA. A comparison of the accuracy of several hip center location prediction methods. J. Biomech. 1990;23:617–621.
[18] Seven YB, Akalan NE, Yucesoy CA. Effects of back loading on the biomechanics of sit-to-stand motion in healthy children. Hum. Movement Sci. 2008;27:65–79.
[19] Kralj A, Jaeger RJ, Munih M. Analysis of standing up and sitting down in humans: definitions and normative data presentation. J. Biomech. 1990;23:1123–1138.
[20] Bader D, Bowker P. Mechanical characteristics of skin and underlying tissues in vivo. Biomaterials. 1983;4:305–308.
[21] Potts RO, Chrisman DA Jr, Buras EM Jr. The dynamic mechanical properties of human skin in vivo. J. Biomech. 1983;16:365–372.
[22] Tepole AB, Gosain AK, Kuhl E. Stretching skin: the physiological limit and beyond. Int. J. Non-Linear Mech. 2012;47:938–949.
[23] Lanir Y, Fung YC. Two-dimensional mechanical properties of rabbit skin-II. Experimental results. J. Biomech. 1974;7:171–182.

[24] Clark JA, Cheng JCY, Leung KS. Mechanical properties of normal skin and hypertrophic scars. Burns. 1996;22:443–446.

[25] Lundström R. Local vibrations-mechanical impedance of the human hand's glabrous skin. J. Biomech. 1984;1:137–144.

[26] Aso M, Yamada Y, Yoshida K, et al. Evaluation of the mechanical characteristics of human thighs for developing complex dummy tissues. In: 2013 IEEE International Conference on Robotics and Biomechanics; Shenzhen; 2013 Dec. p. 1450–1455.